International Journal of Control, Automation and Systems 19(11) (2021) 3753-3763
http://dx.doi.org/10.1007/s12555-020-0959-7
ISSN:1598-6446 eISSN:2005-4092
http://www.springer.com/12555

# Admittance Force Tracking Control Schemes for Robot Manipulators under Uncertain Environment and Dynamics

**Seul Jung*** and **Do-Jin Jeong**

**Abstract:** Force control for robot manipulators is increasingly demanded for stable and desired interaction between robots and environments. In this paper, several modifications of an admittance force control scheme are presented and derived from force tracking impedance functions to give a force tracking capability to position-controlled robot manipulators. Admittance force control known as the position-based force control has a structural advantage of easy implementation for the force control capability to the existing position-controlled robot systems by closing an outer force control loop. The admittance filter as an inverse of impedance function is implemented to filter force errors to modify the reference position such that the eventual force tracking impedance control is realized indirectly. Admittance filters are formulated from impedance functions that guarantee the desired force/position tracking performances with the help of the time-delayed controller. Desired contact force/position tracking control is achieved under uncertain environment and dynamics. Extensive simulation studies of force/position tracking control performances of the proposed control schemes for a robot manipulator are conducted to confirm the proposition.

**Keywords:** Admittance control, force tracking control, impedance control, robot manipulators, time-delayed control.

## 1. INTRODUCTION

Recently, the work domain of robots is rapidly moving from industries to our living environment. The corresponding robots called as collaborative robots are designed to be small to match human arms to fit the environment. Accordingly, robot technologies of collaborative robots for our life domain require more sophisticated control algorithms to deal with interaction with humans more frequently and safely.

Above all, the safety issue is the first priority to be taken into consideration such that collision protection mechanism is required in collaborative robots [1]. Each joint of the robot is equipped with a joint torque sensor to detect the contact force with humans and to minimize the contact force [2]. Learning-based collision detection for collaborative robots was presented [3,4].

Therefore, in order for robots to work properly with humans, not only collision detection methods but also force control methods are required to regulate the contact force and position tracking for stable and desired interaction. Those tasks in the constrained space for robots to perform tasks with environments have to deal with not only position but also contact force.

Force control of industrial robot manipulators has been well developed and utilized for real applications such as grinding, polishing, welding, and assembling parts for a long time.

Two major force control schemes, hybrid force control [5] and impedance force control [6] have been dominantly used. Hybrid force control (HFC) minimizes the force error directly by forming force error equations in force-controlled directions while position is controlled separately. Impedance force control (IFC) regulates the contact force indirectly by controlling the impedance parameters based on the dynamic relationship between the robot and the environment.

Since each control scheme has advantages and disadvantages, a combined control structure known as a hybrid impedance force control (HIFC) has been proposed to have both advantages. HIFC can be configured by giving a direct force tracking capability to impedance force control [7].

In the framework of HIFC, giving a force tracking capability to IFC yields the nonlinear force tracking impedance function [8]. Adding a force error to IFC directly yields

Manuscript received December 21, 2020; revised February 1, 2021, April 2, 2021, and May 16, 2021; accepted June 19, 2021. Recommended by Editor Fumitoshi Matsuno. This paper was supported by the National Research Foundation of Korea under the grant (2017K1A3A1A68072072 & 2019R1I1A3A01062567) and Korea Institute for Advancement of Technology (P0008473, HRD Program for Industrial Innovation).

Seul Jung and Do-Jin Jeong are with the Department of Mechatronics Engineering, Chungnam National University, 99 Daehak-ro, Yuseong-gu, Daejeon 34134, Korea (e-mails: jungs@cnu.ac.kr, woolojuve@naver.com).
* Corresponding author.

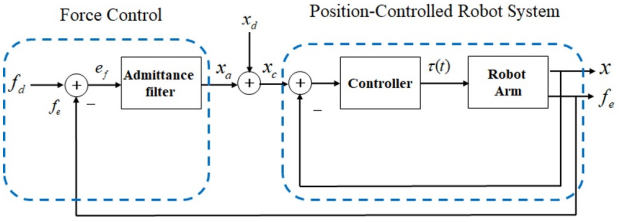


Fig. 1. Concept of a position-based force control scheme.

the force tracking impedance function. By giving infinite compliance, a simple impedance function has been proposed to take care of unknown environment and accurate force tracking performances [9].

In another aspect, the same impedance force control concept can be achieved explicitly by adding an outer force filtering loop. The admittance filter, as an inverse of an impedance filter, can be implemented to filter the force error to generate adjustable position signals. This is configured as a position-based impedance control structure, namely admittance force control [10]. Admittance force control has a structural advantage of giving a force control capability to existing position-controlled robot manipulators without modifying the internal structure as shown in Fig. 1 [11–15]. The admittance filtered signal $x_a$ from a force error $e_f$ plays a role of a hybrid impedance force control function [16].

Therefore, our contribution here is to propose admittance filters derived from the force tracking impedance functions. Force and position tracking performances of several impedance functions are analyzed. The corresponding admittance filters are designed in nonmodel-based configuration to guarantee force/position tracking performances under uncertain environment and dynamics with the help of the time-delayed control (TDC) method [17–20]. Besides TDC, other compensation approaches have been presented as well [21–23].

Extensive simulation studies of force/position tracking control performances for a robot manipulator are conducted to confirm the proposal.

## 2. MODEL-BASED CONTROL IN THE CARTESIAN SPACE

### 2.1. Robot dynamics in the constrained space

The dynamics of an $n$ joint position-controlled robot is described by

$$D(q)\ddot{q}+C(q,\dot{q})+G(q)+\tau_u=\tau, \tag{1}$$

where $D(q)$ is the $n\times n$ inertia matrix, $C(q,\dot{q})$ is the $n\times 1$ Coriolis and centrifugal torque vector, $G(q)$ is the $n\times 1$ gravity force vector, $q$ is the $n\times 1$ joint angle vector, $\dot{q}$ is the $n\times 1$ joint velocity vector, $\ddot{q}$ is the $n\times 1$ joint acceleration vector, $\tau_u$ is the $n\times 1$ nonmodel uncertain torque vector, and $\tau$ is the $n\times 1$ input torque vector.

The Jacobian relationship is given by

$$\dot{X}(t)=J(q)\dot{q}(t), \tag{2}$$

where $J(q)$ is the $n\times n$ Jacobian matrix. The Cartesian acceleration is obtained by differentiating (2) as

$$\ddot{X}(t)=\dot{J}(q)\dot{q}(t)+J(q)\ddot{q}(t). \tag{3}$$

From (3), we have the joint acceleration as

$$\ddot{q}(t)=J^{-1}(\ddot{X}(t)-\dot{J}(t)\dot{q}(t)). \tag{4}$$

Substituting (4) into (1) yields the Cartesian dynamics equation as

$$D^*(t)\ddot{X}(t)+C^*(t)+G^*(t)+F_u(t)=F(t), \tag{5}$$

where $D^*(t)=J^{-T}D(q)J^{-1}$ is the $n\times n$ Cartesian inertia matrix, $C^*(t)=-J^{-T}D(q)J^{-1}\dot{J}J^{-1}\dot{X}+J^{-T}C(q,\dot{q})$ is the $n\times 1$ Cartesian Coriolis and centrifugal force vector, $G^*(t)=J^{-T}G(q)$ is the $n\times 1$ Cartesian gravity force vector, $X(t)$ is the $n\times 1$ position vector, $\dot{X}(t)$ is the $n\times 1$ linear velocity vector, $\ddot{X}(t)$ is the $n\times 1$ linear acceleration vector, $F_u$ is the $n\times 1$ nonmodel force vector, and $F$ is the $n\times 1$ input force vector.

For simplicity, (5) can be described as a simplified form as

$$D^*(t)\ddot{X}(t)+h^*(t)=F(t), \tag{6}$$

where $h^*(t)=C^*(t)+G^*(t)+F_u(t)$.

### 2.2. Model-based position control in the constrained space

The model-based feedback linearization provides the control law as

$$F(t)=\hat{D}^*(t)V(t)+\hat{h}^*(t), \tag{7}$$

where $\hat{D}^*$, $\hat{h}^*$ are estimates of $D^*$, $h^*$ and $V(t)$ is the Cartesian control input to minimize the Cartesian position error $e(t)$ as

$$V(t)=\ddot{X}_d(t)+K_D\dot{e}(t)+K_Pe(t), \tag{8}$$

where $e(t)=X_d(t)-X(t)$ and $X_d(t)$ is the desired trajectory and $X(t)$ is the actual trajectory.

Combining (7) and (8) with (6) yields the closed loop error equation as

$$\ddot{e}(t)+K_D\dot{e}(t)+K_Pe(t)=\hat{D}^{*-1}(t)(\Delta\hat{D}^*(t)\ddot{X}(t)+\Delta\hat{h}^*(t)), \tag{9}$$

where $K_D$, $K_P$ are controller gain matrices and robot dynamic model uncertainties are given as

$$\Delta\hat{D}^*(t)=D^*(t)-\hat{D}^*(t),\Delta\hat{h}^*(t)=h^*(t)-\hat{h}^*(t), \tag{10}$$

which are required to be compensated by the time-delayed controller (TDC) in this paper. Then we have the perfect position tracking independently.

$$\ddot{e}(t) + K_D\dot{e}(t) + K_P e(t) = 0. \tag{11}$$

If uncertainties in (9) are not fully compensated, then position tracking performance is not guaranteed.

## 3. TIME-DELAYED CONTROL

The time-delayed control is a nonmodel-based robust control scheme that guarantees tracking performances by compensating for uncertainties in internal dynamics and outer disturbances. Robot dynamics equation (1) can be reformulated with the constant inertia matrix $\bar{D}$ as

$$\bar{D}\ddot{q}(t) + \bar{h}(t) = \tau(t), \tag{12}$$

where $\bar{D} = \alpha I$ and $\alpha$ is a constant, and $\bar{h}(t) = D(q)\ddot{q}(t) - \bar{D}\ddot{q}(t) + C(q,\dot{q}) + G(q) + \tau_u$.

The idea of the time-delayed control scheme is to use the previous control information to estimate the uncertainty $\bar{h}(t)$ in (12). Based on the dynamics of (12), uncertainty $\bar{h}(t)$ can be estimated with other information, $\bar{D}$, $\ddot{q}(t)$, and $\tau(t)$ such that

$$\bar{h}(t) = \tau(t) - \bar{D}\ddot{q}(t). \tag{13}$$

However, $\bar{h}(t)$ is not available from $\ddot{q}(t)$, $\tau(t)$ at the same time $t$. Therefore, TDC uses the previously sampled information to approximate $\bar{h}(t)$ as $\hat{\bar{h}}(t)$.

$$\hat{\bar{h}}(t) \cong \bar{h}(t-T) = \tau(t-T) - \bar{D}\ddot{q}(t-T), \tag{14}$$

where $T$ is the sampling time and this approximation requires the fast sampling time to ignore the time delay effect.

Then a nonmodel TDC law in the joint space becomes

$$\tau(t) = \bar{D}u(t) + \hat{\bar{h}}(t), \tag{15}$$

where the control input $u(t)$ is represented with the joint acceleration $\ddot{q}(t)$ in the joint space.

For the Cartesian space control, we have the transformation relationship with the joint space as

$$\ddot{q}(t) = u(t) = J^{-1}(V(t) - \dot{J}\dot{q}(t)). \tag{16}$$

Combining (14), (15), and (16) yields the TDC control law as

$$\tau(t) = \bar{D}J^{-1}(V(t) - \dot{J}\dot{q}(t)) + \tau(t-T) - \bar{D}\ddot{q}(t-T). \tag{17}$$

In order to realize TDC in (17), $\bar{D}$ and $\ddot{q}(t)$ are required along with the control torque information at the previous sampling time, $\tau(t-T)$. An alternative way is to use Jacobian transpose to realize the TDC control law as

$$\tau(t) = \bar{D}K_t J^T V(t) + \tau(t-T) - \bar{D}\ddot{q}(t-T), \tag{18}$$

where $K_t$ is a torque constant matrix.

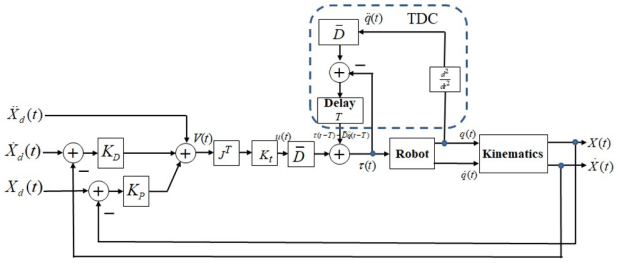


Fig. 2. TDC scheme for position control in the Cartesian space.

The Cartesian TDC block diagram is shown in Fig. 2. The fast sampling time can be achieved by choosing the appropriate hardware such as DSPs, and the accurate acceleration estimation of $\ddot{q}(t)$ can be achieved by designing appropriate filters for signals from sensors.

## 4. ADMITTANCE CONTROL

### 4.1. Original impedance function

Impedance force control regulates the contact force indirectly by adjusting the impedance parameters between the applied force exerted by a robot and the constrained velocity/position by an object [2].

Impedance force control has been developed to have the force tracking capability from the original impedance function by Hogan [3,4].

The original impedance function is defined as

$$f_{ext}(t) = m\ddot{e}_x(t) + b\dot{e}_x(t) + ke_x(t), \tag{19}$$

where $f_{ext}$ is the exerted force, $e_x = x_d - x$, and $m$, $b$, $k$ are impedance parameters. Specifying the desired position $x_d$ appropriately in association with environment position $x_e$, the effective stiffness $k_{eff}$, and the desired force $f_d$ yields the force tracking performance. The desired position can be specified as

$$x_d(t) = x_e(t) + \frac{f_d(t)}{k_{eff}}, \tag{20}$$

where $k_{eff} = \frac{kk_e}{k+k_e}$ and $k$ is a stiffness parameter and $k_e$ is the environment stiffness, which means that desired force tracking control can be done with the exact environment information of $k_e$ and $x_e$ to determine the exerted force on the environment, which is impractical. Therefore, the original impedance function lacks in the force tracking capability.

### 4.2. Scheme 1: Force tracking impedance function

To give the force tracking capability to (19), a force tracking impedance function has been suggested by specifying the desired force directly and redefining the positional error as

$$f_{ext}(t) - f_d(t) = m\ddot{\varepsilon}(t) + b\dot{\varepsilon}(t) + k\varepsilon(t), \tag{21}$$

where the position error is defined as $\varepsilon(t) = x_e(t) - x(t)$.

Equation (21) forms the hybrid impedance force function with the force tracking error function. Note that the contact force is defined as

$$f_{ext}(t) = -k_e\varepsilon(t) = k_e(x(t) - x_e(t)). \tag{22}$$

From (22), substituting $\varepsilon(t) = -\frac{f_{ext}(t)}{k_e}$ into (21) yields the function with force terms as

$$k_e(f_{ext}(t) - f_d(t)) = -(m\ddot{f}_{ext}(t) + b\dot{f}_{ext}(t) + kf_{ext}(t)). \tag{23}$$

Arranging (23) yields

$$k_e f_d(t) = m\ddot{f}_{ext}(t) + b\dot{f}_{ext}(t) + (k + k_e)f_{ext}(t). \tag{24}$$

Laplace transform of (24) provides the relationship between the desired force $f_d(s)$ and the actual force $f_{ext}(s)$ as

$$\frac{f_{ext}(s)}{f_d(s)} = \frac{k_e}{ms^2 + bs + (k + k_e)}. \tag{25}$$

Final value theorem for the desired step force command $f_d(s) = 1/s$ gives us that the actual force has the magnitude of $f_{ext}(\infty) = \frac{k_e}{k+k_e} f_d(t)$.

$$\lim_{s\to 0} f_{ext}(s) = \lim_{s\to 0} s\frac{k_e}{ms^2 + bs + (k + k_e)} f_d(s) = \frac{k_e}{k + k_e}. \tag{26}$$

In reality, a stiff environment shows $k_e >> k \to f_{ext}(\infty) \approx f_d$, which follows the desired force. However, the force tracking error becomes larger for the low stiffness environment.

In the same way, we have the positional error at the convergence as

$$\frac{\varepsilon(s)}{f_d(s)} = -\frac{1}{ms^2 + bs + (k + k_e)}. \tag{27}$$

The position tracking error in the force-controlled direction becomes

$$\lim_{s\to 0}\varepsilon(s) = \lim_{s\to 0}(-\frac{1}{ms^2 + bs + (k + k_e)})\frac{1}{s} = -\frac{1}{k + k_e}, \tag{28}$$

which is $x_e(\infty) - x(\infty) = -\frac{1}{k+k_e}$.

This means that position tracking in the force controlled direction always results in errors to guarantee the force tracking performance. Thus depending upon the values of $k$ and $k_e$, the positional error can be minimized to achieve position tracking performance in the force-controlled direction as well.

For the admittance filter, taking the inverse of the impedance filter from (21), Laplace transform of (21) yields the impedance function between a force error and a position error. Defining the force error as $e_f(s) = f_d(s) - f_{ext}(s)$ yields

$$e_f(s) = -(ms^2 + bs + k)\varepsilon(s). \tag{29}$$

The position modifying term can be defined from (29) as

$$x_a(s) = \frac{k_a}{ms^2 + bs + k} e_f(s), \tag{30}$$

where $k_a$ is the filter adjusting gain. The position modifying term is added to the reference trajectory $x_d$, which is the estimation of $x_e$ in the force-controlled direction. For the position-controlled direction, positional errors are minimized as usual.

As a result, since the force tracking impedance function in (21) does not guarantee both force and position tracking performances, the admittance filter based on (21) is expected to have the same force errors in the force-controlled direction.

### 4.3. Scheme 2: Simplified impedance function

Next is to present a further simplified force tracking impedance function by letting the impedance stiffness gain $k = 0$ to give infinite compliance to the relation such that (21) for the force-controlled direction becomes

$$f_{ext}(t) - f_d(t) = m\ddot{\varepsilon}(t) + b\dot{\varepsilon}(t). \tag{31}$$

From (22), substituting $\varepsilon(t) = -\frac{f_{ext}(t)}{k_e}$ into (31) yields

$$k_e(f_{ext}(t) - f_d(t)) = -(m\ddot{f}_{ext}(t) + b\dot{f}_{ext}(t)). \tag{32}$$

Arranging (32) yields

$$k_e f_d(t) = m\ddot{f}_{ext}(t) + b\dot{f}_{ext}(t) + k_e f_{ext}(t). \tag{33}$$

Laplace transform of (33) provides the relationship between the desired force and the actual force as

$$\frac{f_{ext}(s)}{f_d(s)} = \frac{k_e}{ms^2 + bs + k_e}. \tag{34}$$

At a steady state, (34) guarantees $f_{ext}(t) = f_d(t)$, which shows the perfect force tracking result.

$$\lim_{s\to 0} f_{ext}(s) = \lim_{s\to 0}(\frac{k_e}{ms^2 + bs + k_e})\frac{1}{s} = 1. \tag{35}$$

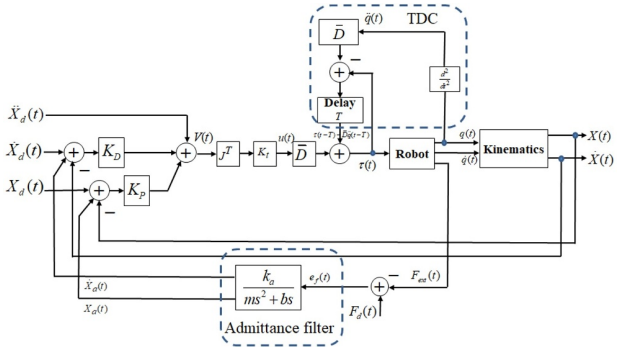


Fig. 3. Position-based contact force control block diagram.

In the same way, we have the positional error at the convergence as

$$\frac{\varepsilon(s)}{f_d(s)} = -\frac{1}{ms^2+bs+k_e}. \tag{36}$$

The position tracking error in the force-controlled direction becomes

$$\lim_{s\to 0}\varepsilon(s) = \lim_{s\to 0}s(-\frac{1}{ms^2+bs+k_e})\frac{1}{s} = -\frac{1}{k_e}, \tag{37}$$

which shows a larger error than (28), but still small due to a division by a large stiffness $k_e$ that results in force control. Simultaneously, position tracking control can be satisfied in the force controlled direction at a certain accuracy given in (37).

The admittance filter for the impedance function is designed as

$$x_a(s) = \frac{k_a}{ms^2+bs}(f_d(s) - f_{ext}(s)), \tag{38}$$

where $k_a$ is the positional adjustment gain. The force tracking error is filtered by the admittance filter in (38) to generate the positional adjustment to modify the reference position to have the force tracking capability indirectly.

The admittance force control block diagram of Scheme 2 is shown in Fig. 3.

## 5. CONTACT FORCE TRACKING CONTROL

### 5.1. Force control environment

Fig. 4 shows the experimental setup. A three-link robot in Table 1 is tested for the force tracking performance on the environment having the stiffness of 30,000 N/m, which is unknown to the robot located at $X_0 = [0.7341, 0, 0.9641]^T$ m. The initial angle of the robot is $q_0 = [0, \pi/4, -\pi/4]^T$. The robot is required to apply 10 N desired force on the environment normal to the $x$ axis while the robot follows the sinusoidal trajectory in the $z$ axis at the same time so that force control in the $x$ axis and position control in the $z$ axis are conducted.

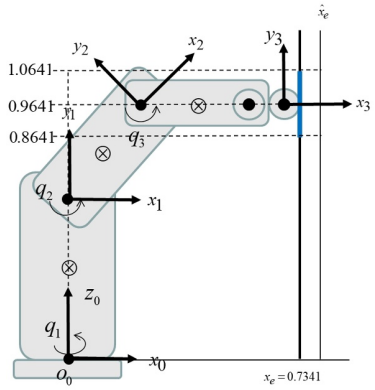


Fig. 4. Environment setup.

Table 1. Robot parameters.

| Joint $i$ | Mass | Length | Friction |
|---|---|---|---|
| 1 | 30 kg | 0.66 m | $3\dot{q}_1 + 5\text{sgn}(\dot{q}_1)$ |
| 2 | 17.4 kg | 0.43 m | $3\dot{q}_2 + 5\text{sgn}(\dot{q}_2)$ |
| 3 | 4.8 kg | 0.43 m | $3\dot{q}_3 + 5\text{sgn}(\dot{q}_3)$ |

### 5.2. Position control

Here we are conducting position control before force control is applied. Three cases are considered.

1) Computed-torque control with 100% models

Since models are perfectly available, position tracking results are also perfect as shown in Fig. 5.

2) Nonmodel-based control with joint frictions

However, when dynamics models are not available, we have poor tracking performances as shown in Fig. 6.

3) TDC scheme

TDC compensates for those uncertainties in Fig. 6 and makes position tracking better as shown in Fig. 7.

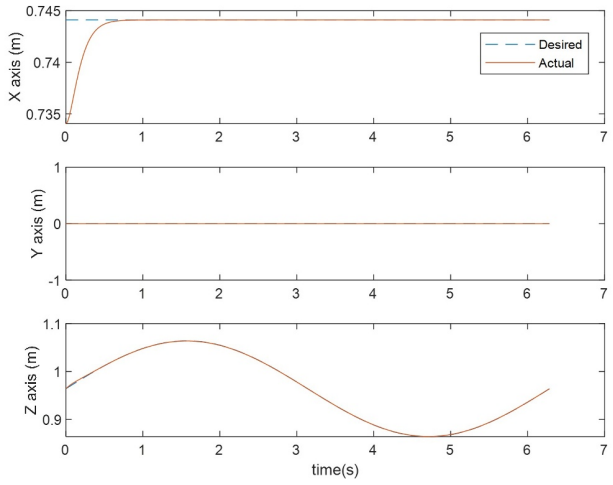


Fig. 5. Position control of model-based control.

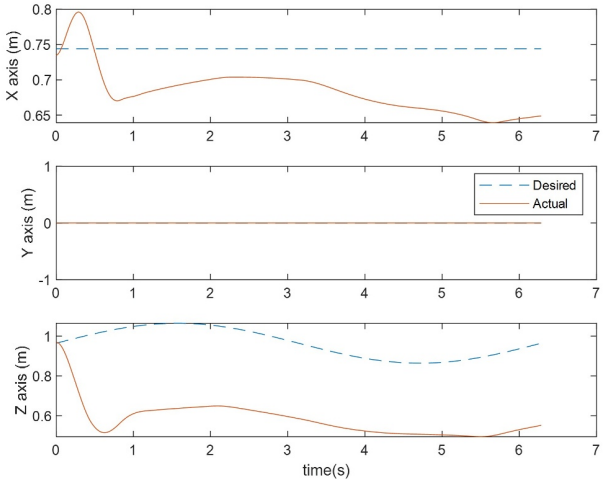


Fig. 6. Position control of nonmodel-based control.

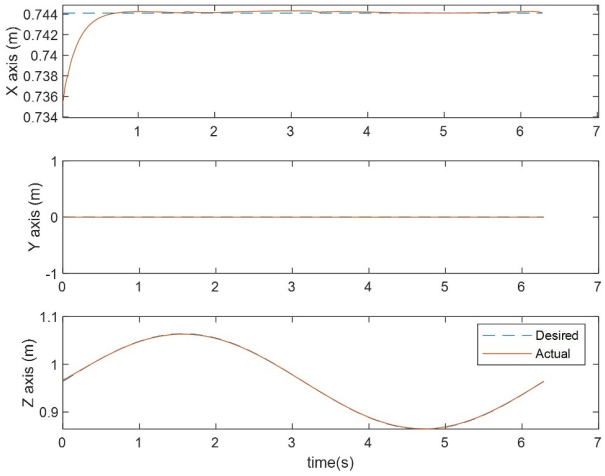


Fig. 7. Position control of TDC.

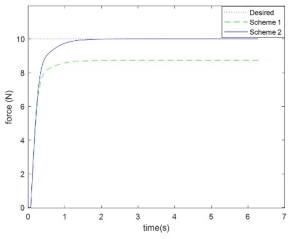


(a) Force tracking.

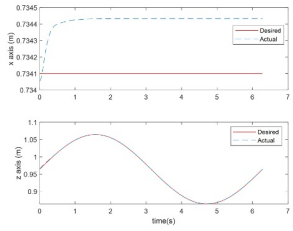


(b) Position tracking of Scheme 2.

Fig. 8. Force control under model-based control $k_a = 0.1$.

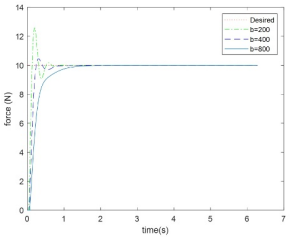


(a) Force tracking.

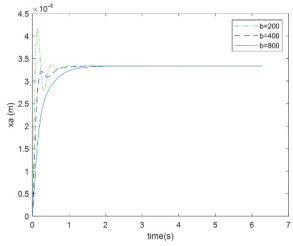


(b) Position adjustment xa.

Fig. 9. Model-based control(Scheme 2): Different damping gains for step command.

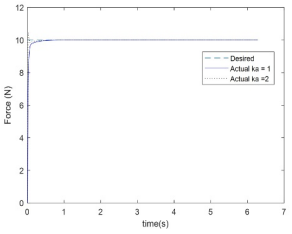


(a) Force tracking.

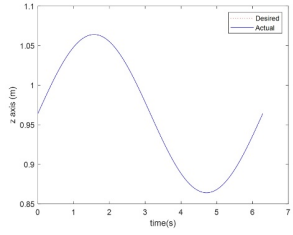


(b) Position tracking of Scheme 2 ($k_a = 1$).

Fig. 10. Force control under model-based control .

### 5.3. Force control under model-based dynamics

1) Step force command

The first task is for a robot to follow the 10N force against the environment while moving up and down as shown in Fig. 4. Admittance force control is conducted under the full model-based control to analyze the performance. Full model-based control means here the computed torque control with the exact models. Since the robot is position-controlled, position controllers are designed as

$$V_P = K_A^{-1}(\ddot{X}_d + K_D(\dot{X}_d - \dot{X}) + K_P(X_d - X)), \qquad (39)$$

where controller gains are selected as $K_A = 0.1I$, $K_D = 20I$, $K_P = 100I$.

The admittance filter of $x_{a1}(s) = \frac{0.1}{s^2+800s+400} e_f(s)$ for Scheme 1 is used. The admittance filter of $x_{a2}(s) = \frac{0.1}{s^2+800s} e_f(s)$ for Scheme 2 is used. We see from Fig. 8(a) the force tracking offset of Scheme 1 due to (26) and no offset of Scheme 2 due to (35). For the root-mean-square (RMS) positional tracking error in the $z$-axis, both schemes show the same error of 0.0370 as shown in Fig. 8(b).

Force tracking tests for different damping gains are conducted. We see from Fig. 9(a) that the force tracking performance by different damping gains of the admittance filter of Scheme 2. Higher damping gain shows the less overshoot, but the slow response. The position modification signals from the admittance filters are also plotted in Fig. 9(b).

The shapes are exactly same as force tracking responses, which means that $x_a$ regulates the force response. Fig. 10 shows the force/position responses when the admittance filter for Scheme 2 is $x_{a2}(s) = \frac{1}{s^2+800s} e_f(s)$ where the adjustable gain is $k_a = 1$. The positional RMS error

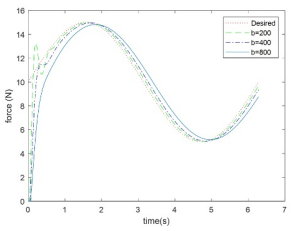


(a) Force tracking.

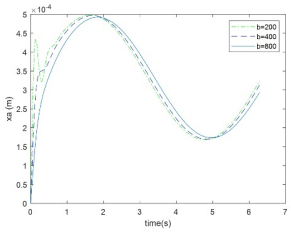


(b) Position adjustment xa.

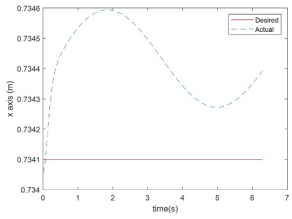


(c) Position in the $x$ aixs.

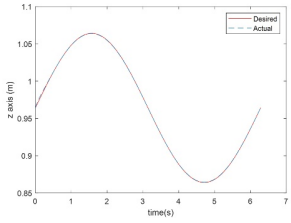


(d) Position tracking in the $z$ axis ($b = 800$).

Fig. 11. Model-based control(Scheme2): Different damping gains for sinusoidal command.

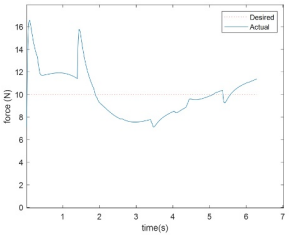


(a) Force tracking.

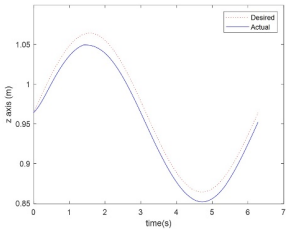


(b) Position tracking.

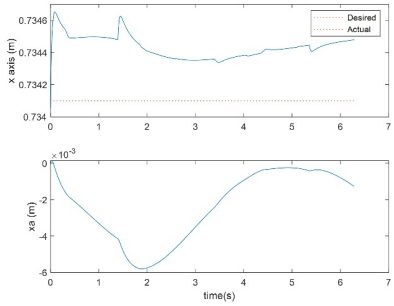


(c) Position in the $x$-axis.

Fig. 12. Nonmodel-based control (Scheme 2).

is further minimized to 0.0016 which is smaller than Fig. 8(b). The gain $k_a = 1$ shows the fast contact compared with Fig. 9(a). Fig. 10 shows the better force response and smaller tracking errors. So the gain can be optimized, but increasing gain $k_a$ further causes a force overshoot. When $k_a = 2$, 0.45% overshoot has been observed in Fig. 10(a).

2) Sinusoidal force command

The force tracking capability is tested. The sinusoidal force is given as $f_d(t) = 10 + 5\sin(t)$ which is shown in Fig. 11(a). The admittance filter $x_{a2}(s) = \frac{0.1}{s^2+bs} e_f(s)$ for Scheme 2 is given. Force tracking responses for different damping gains, $b = 200$, 400, 800 are plotted in Fig. 11(a). As the damping gain is larger, force overshoot is minimized, but time delay also becomes larger. The RMS errors of position tracking for all cases are same as 0.0370, which means that force-controlled direction and position-controlled direction are decoupled. Fig. 11(b) shows the modification signals from the admittance filters. As expected, signals are same patterns with force response shown in Fig. 11(a), which regulates the contact forces. Figs. 11(c) and 11(d) show position tracking results in the $x$-axis and $z$-axis, respectively.

## 5.4. Force control under nonmodel-based dynamics

In most of cases, it is true that full dynamics models are not available and additional friction terms are present. As a result, the performances of nonmodel-based force tracking control are degraded.

1) Step force command

Similar tasks are tested. Scheme 2 uses the admittance filter of $x_{a2}(s) = \frac{1}{s^2+800s} e_f(s)$. The positional RMS error is 3.2052 which is much larger. Fig. 12(a) shows the force tracking response corrupted by joint friction and nonmodel dynamics. The corresponding position plot also shows the notable errors in Fig. 12(b). The modifying term from the admittance filter $x_a$ in Fig. 12(c) below does not follow Fig. 12(a) due to uncertainties.

2) Sinusoidal force command

The sinusoidal force is also tested. The positional RMS error is 3.2052 m which is same as Fig. 12. Similarly the force/position tracking results show notable errors in Figs. 13(a) and 13(b), respectively. Although the modifying signals $x_{a1}$, $x_{a2}$ for Figs. 12(c) and 13(c) look similar, there is a difference in a small scale.

## 5.5. Force control under nonmodel dynamics with TDC

1) Step force command

For a constant inertia model, we have used $\bar{D} = 0.1I$. Same tasks are conducted with TDC. The positional RMS error is 0.0044, which is much reduced. Force/position tracking performances are significantly improved as shown in Figs. 14(a) and 14(b). Small periodic force errors are still there, but the error is much small compared with Fig. 12(a). Fig. 14(d) shows the joint torques for each joint.

2) Step force command with different environment stiffness

Given the similar condition such as the admittance filter of $x_{a2}(s) = \frac{1}{s^2+800s} e_f(s)$ and gains of $K_A = 5I, K_D = 20I, K_P = 100I$ with the torque constant of 200, three different environment stiffness are tested as $k_e = 10000, 50000, 100000(N/m)$. Step force tracking re-

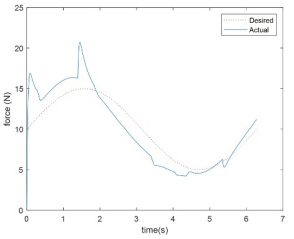


(a) Force tracking.

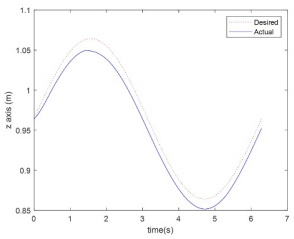


(b) Position tracking.

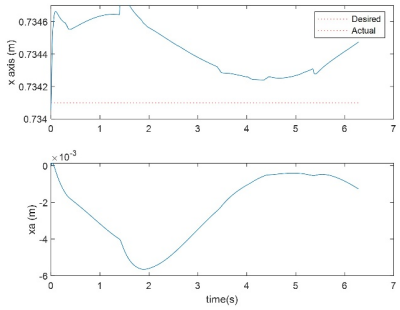


(c) Position in the $x$-axis.

Fig. 13. Nonmodel-based control(Scheme 2).

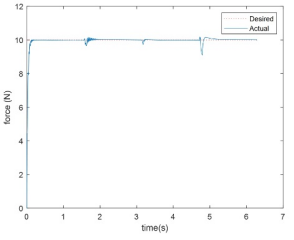


(a) Force tracking.

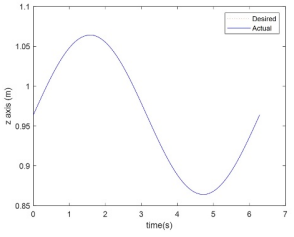


(b) Position.

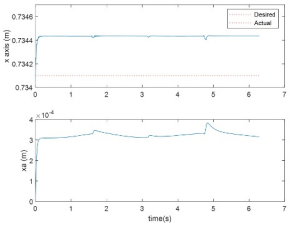


(c) Position in the $x$-axis.

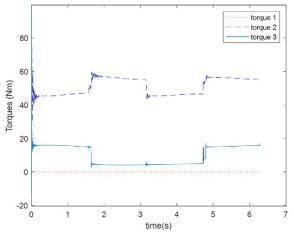


(d) Joint torques.

Fig. 14. Nonmodel-based control with TDC (Scheme 2).

sults are compared in Fig. 15(a) and the corresponding force errors are shown in Fig. 15(b) to compare more clearly. Fig. 15(c) shows the position tracking results, which show similarly good tracking performances.

3) Sinusoidal force command

Sinusoidal force tracking response is shown in Fig. 16(a), which shows the same periodic force errors as Fig. 14(a) due to the joint frictions. Positional RMS error is 0.0044, which is same as Fig. 14(b). This means that

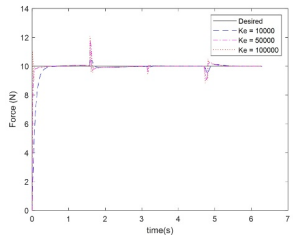


(a) Step force.

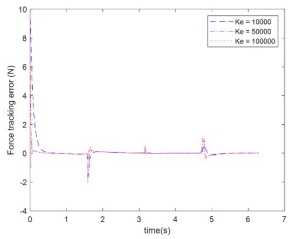


(b) Force errors.

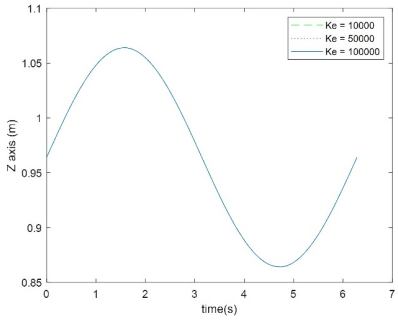


(c) Position tracking in the $z$-axis.

Fig. 15. Nonmodel-based control with TDC for different environment stiffness.

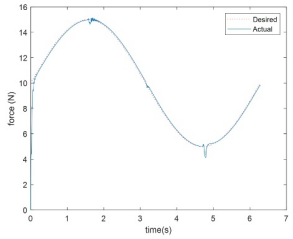


(a) Force tracking.

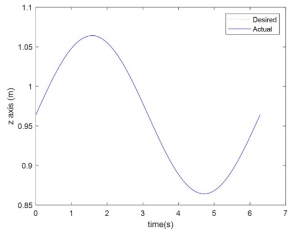


(b) Position.

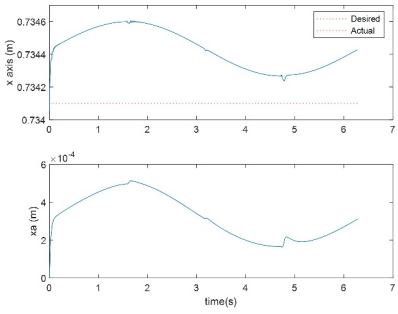


(c) Position in the $x$-axis.

Fig. 16. Nonmodel-based control with TDC (Scheme 2).

force/position are controlled separately because we see different force tracking results between Fig. 13(a) and Fig 16(a). In most of cases, it is true that full models are not available.

4) Sinusoidal force command with different environment stiffness

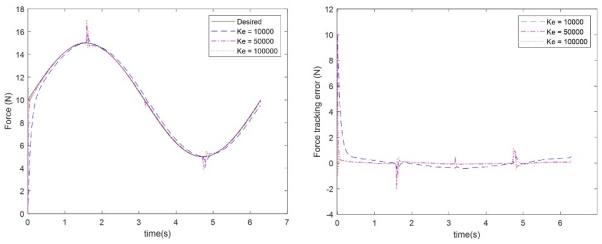


(a) Sinusoidal force. (b) Force errors.

Fig. 17. Nonmodel-based control with TDC for different environment stiffness.

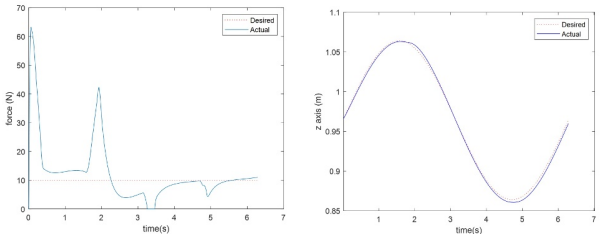


(a) Force tracking. (b) Position tracking.

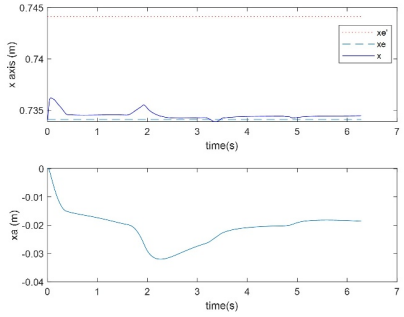


(c) $X$-axis position.

Fig. 18. Scheme 2 without TDC.

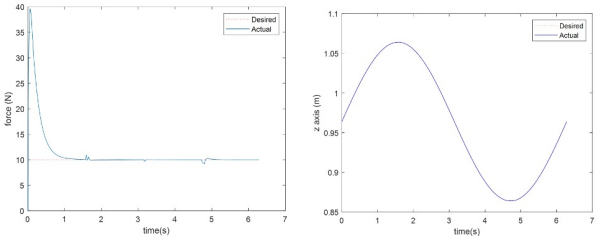


(a) Force. (b) Position.

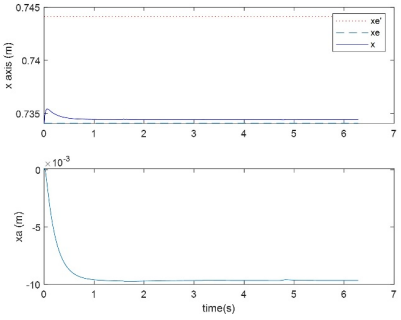


(c) $X$-axis position.

Fig. 19. Scheme 2 with TDC.

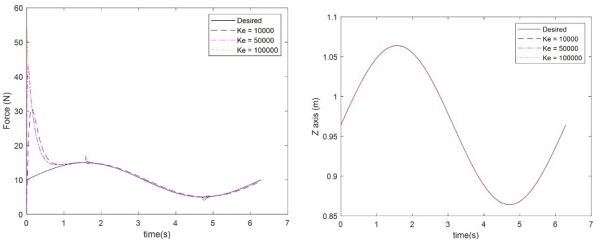


(a) Force tracking. (b) $Z$-axis position.

Fig. 20. Nonmodel-based control with TDC for different environment stiffness with environment position error.

Fig. 17 shows the sinusoidal force tracking results. As the stiffness increases, force overshoot is increased. For the clear comparison, force tracking errors are plotted in Fig. 17(b).

## 5.6. Force control with environment position error

Next is to test uncertainty effect of the environment position error on the force/position tracking performances. The environment position is assumed to have an error of 0.01 m such that $\hat{x}_e = x_e + 0.01$ m. Under uncertainties in dynamics, Scheme 2 is tested with TDC and without TDC.

1) Step force command without TDC

Fig. 18 shows the tracking responses due to uncertainties in both the environment and the dynamics. As expected, the initial contact force overshoot is over 60 N and the tracking results are not good as shown in Fig. 18(a). The corresponding position tracking error in the $z$ axis is shown in Fig. 18(b). The correction signal from the admittance filter is shown in Fig. 18(c).

2) Step force command with TDC

Fig. 19 shows the tracking responses by TDC. The initial contact force overshoot is reduced to 40 N and force tracking is better than Fig. 19(a). The corresponding position tracking of the $z$-axis shown in Fig. 19(b) is also better. The correction signal from the admittance filter in Fig. 19(c) follows the shape of the force response in Fig. 19(a). To minimize the overshoot force, the accurate estimation of the environment position is required.

3) Sinusoidal force command with TDC for different environment stiffness

Finally, force tracking performances for different stiffness with environment position error were tested. Fig. 20 shows the tracking results. We see clearly from Fig. 20(a) that contact force overshoot is larger as the stiffness in-

creases from 30 N to 55 N. However, the force tracking response after contact is good as well as position tracking in the $z$ axis.

## 6. CONCLUSIONS

The admittance force control schemes for robot manipulators have been presented on the basis of the analysis from the impedance force control functions. The admittance force control schemes guarantee force/position tracking performances under uncertain environment and dynamics with the help of the time-delayed controller. Simulation studies have shown the guaranteed force tracking performance based on appropriately selecting filter coefficients under unknown environment stiffness and position. The feasibility of the admittance filtering technique can be applied to real position-controlled robot manipulators without having a force control capability. Developing algorithms of minimizing the force overshoot of a robot manipulator at the initial contact from free space are required in the future research.

## REFERENCES


[1] W. Li, Y. Han, J. Wu, and Z. Xiong, "Collision detection of robots based on a force/torque sensor at the bedplate," *IEEE/ASME Trans. on Mechatronics*, vol. 25, no. 5, pp. 2565-2573, 2020.

[2] Y. Lou, J. Wei, and S. Song, "Design and optimization of a joint torque sensor for robot collision detection," *IEEE Sensor Journal*, vol. 19, no. 16, pp. 6618-6627, 2019.

[3] Y. J. Heo, D. Y. Kim, W. Lee, H. K. Kim, J. H. Park, and W. K. Chung, "Collision detection for industrial collaborative robots: A deep learning approach," *IEEE Robots and Automation Letters*, vol. 4, no. 2, pp. 740-746, 2019.

[4] K. M. Park, J. H. Kim, J. H. Park, and F. C. Park, "Learning-based real-time detection of robot collisions without joint torque sensors," *IEEE Robots and Automation Letters*, vol. 6, no. 1, pp. 103-110, 2019.

[5] M. Raibert and J. J. Craig, "Hybrid position/force control of manipulators," *ASME Journal. of Dynamic Systems, Measurements, and Control*, vol. 102, pp. 126-133, 1981.

[6] N. Hogan, ''Impedance control: An approach to manipulator, Part i, ii, iii," *ASME Journal of Dynamics Systems, Measurements, and Control*, vol. 3, pp. 1-24, 1985.

[7] R. J. Anderson and M. W. Spong, "Hybrid impedance control of robot manipulators," *IEEE Journal of Robotics and Automation*, vol. 4, no. 5, pp. 549-556, 1988.

[8] S. Jung, T. C. Hsia, and R. G. Bonitz, "Force tracking impedance control for robot manipulators with an unknown environment: Theory, simulation, and experiment," *The International Journal of Robotics Research*, vol. 20, no. 9, pp. 765-774, 2001.

[9] S. Jung, T. C. Hsia, and R. G. Bonitz, "Force tracking impedance control of robot manipulators under unknown environment," *IEEE Trans. on Control Systems Technology*, vol. 12, no. 3, pp. 474-483, 2004.

[10] S. Jung, "A position-based force control approach to a quad-rotor system," *URAI*, pp. 373-377, 2012.

[11] H. Seraji, "Adaptive admittance control: An approach to explicit force control in compliant motion," *Proc. IEEE Conference on Robotics and Automations*, pp. 2705-2712, 1994.

[12] Q. Yang, J. Niu, and R. Song, "Admittance control of a 3 DOF cable-driven rehabilitation robot for upper-limb in three dimensional workspace," *ICARM*, pp. 445-449, 2017.

[13] E. E. Cruz and W. Y. Liu, "Stable PD position/force control in bidirectional teleoperation," *Proc. of International Conference on Electrical Engineering, Computing Science and Automatic Control*, 2018.

[14] Z. Li, B. Huang, Z. Ye, M. Deng, and C. Yang, "Physical human-robot interaction of a robotic exoskeleton by admittance control," *IEEE Trans. on Industrial Electronics*, vol. 65, no. 12, pp. 9614-9624, 2018.

[15] G. Kang, H. S. Oh, J. K. Seo, U. Kim, and H. R. Choi, "Variable admittance control of robot manipulators based on human intention," *IEEE/ASME Trans. on Mechatronics*, vol. 24, no. 3, pp. 1023-1032, 2019.

[16] S. Jung, "Admittance force tracking control for position-controlled robot manipulators under unknown environment," *ICCAS*, pp. 219-224, 2020.

[17] T. C. Hsia, "On a simplified joint controller design for robot manipulators," *Proc. of IEEE Conf. on CDC*, pp. 1024-1025, 1987.

[18] K. Yousef-Toumi and O. Ito, "A time-delay controller for systems with unknown dynamics," *Journal of Dynamic Systems, Measurement, and Control*, vol. 112, pp. 133-142, 1990.

[19] P. H. Chang and S. H. Park, "On improving time-delay control under certain hard nonlinearities," *Mechatronics*, vol. 13, pp. 393-412, May 2003.

[20] S. U. Lee and P. H. Chang, "The development of anti-windup scheme for time delay control with switching action using integral sliding surface," *Trans. ASME J. Dyn. Syst. Meas. Control*, vol. 125, no. 4, pp. 630-638, Dec. 2003.

[21] S. Jung, "Stability analysis of reference compensation technique for controlling robot manipulators by neural network," *International Journal of Control, Automation, and Systems*, vol. 15, no. 2, pp. 952-958, 2017.

[22] S. Jung, "Improvement of tracking control of a sliding mode controller for robot manipulators by a neural network," *International Journal of Control, Automation, and Systems*, vol. 16, no. 2, pp. 937-943, 2018.

[23] Y. G. Bae and S. Jung, "Balancing control of a mobile manipulator with two-wheels by an acceleration-based disturbance observer," *International Journal of Humanoid Robotics*, vol. 15, no. 3, 2018.

**Seul Jung** received his B.S. degree in electrical and computer engineering from Wayne State University, Detroit, MI, USA in 1988, and his M.S. and Ph.D. degrees in electrical and computer engineering from the University of California, Davis in 1991 and 1996, respectively. In 1997, he joined the Department of Mechatronics Engineering, Chungnam National University, where he is presently a professor. His research interests include intelligent mechatronics systems, intelligent robotic systems, autonomous navigation, gyroscope applications, and robot education.

**Do-Jin Jeong** received his B.S. degree in mechanical engineering from Han Nam University in 2019. He is currently a graduate student for a master degree at Department of Mechatronics Engineering at Chungnam National University. His research interests are mechatronic system modeling, control moment gyroscope and force control.